Passive Q-switching of Yb bulk lasers by a graphene saturable absorber

P.A. Loiko[1,2], J.M. Serres[1], X. Mateos[1,3,*], J. Liu[4], H. Zhang[5], A.S. Yasukevich[2], K.V. Yumashev[2], V. Petrov[3], U. Griebner[3], M. Aguiló[1] and F. Díaz[1]

[1]Física i Cristal·lografia de Materials i Nanomaterials (FiCMA-FiCNA), Universitat Rovira i Virgili (URV), Campus Sescelades, c/ Marcel·lí Domingo, s/n., Tarragona, Spain E-43007
[2]Center for Optical Materials and Technologies, Belarusian National Technical University, 65/17 Nezavisimosti Ave., Minsk, Belarus 220013
[3]Max Born Institute for Nonlinear Optics and Short Pulse Spectroscopy, 2A Max-Born-Str., Berlin, Germany D-12489
[4]College of Physics, Qingdao University, 308 Ning-Xia Road, Qingdao, China 266071
[5]State Key Laboratory of Crystal Materials and Institute of Crystal Materials, Shandong University, Jinan, China 250100

*e-mail: xavier.mateos@urv.cat, mateos@mbi-berlin.de

Abstract Compact Yb:$KLu(WO_4)_2$ and Yb:$LuVO_4$ lasers diode-pumped at 978 nm are passively Q-switched by a single-layer graphene saturable absorber. The Yb:$KLu(WO_4)_2$ laser generated 165 ns / 0.49 μJ pulses at 1030 nm with 170 mW average output power and 12% slope efficiency. With the Yb:$LuVO_4$ laser, 152 ns / 0.83 μJ pulses were achieved. The output power reached 300 mW at 1024 nm and the slope efficiency was 10%. Laser operation in a plano-plano cavity is achieved with both crystals with thermal lensing playing a key role in their performance. A model describing graphene Q-switched Yb lasers is developed. Our results indicate the potential of graphene for passive Q-switching of ~1 μm bulk lasers.

PACS: 81.05.ue; 42.55.Xi; 42.60.Gd; 42.70.Hj

1. Introduction

The Ytterbium ion (Yb^{3+}) is attractive for laser operation near 1 μm ($^2F_{5/2} \rightarrow {}^2F_{7/2}$ transition). Yb lasers can be pumped with commercial high-power InGaAs laser diodes emitting at 930 – 980 nm. The simple energy level scheme of the Yb^{3+} ion and the associated absence of parasitic processes like up-conversion and excited-state absorption lead to a low heat loading and exceptionally high slope efficiencies (>80%). In addition, some tuning of the laser wavelength is also possible with Yb lasers, similar to vibronic transition metal lasers.

In recent years, two crystal families attracted attention for Yb^{3+} doping, these are the monoclinic double tungstates, $KRE(WO_4)_2$ [1] and tetragonal vanadates, $REVO_4$ [2,3] (where RE stands for a "passive" element like Gd, Y or Lu). Both crystal families offer attractive spectroscopic properties [1,2], in particular highest absorption and stimulated-emission cross- sections (among the known hosts for Yb^{3+} ions) with a strong polarization-anisotropy and relatively broad emission bands. $REVO_4$ crystals are characterized with good thermal [4] and thermo-optical properties [5] that can compete with YAG. The feature of $KRE(WO_4)_2$ host is the large dopant ion-ion separation which enables doping with Yb^{3+} ions at very high concentrations [6] that enables engineering of various geometries of the active medium [7,8]. Among "passive" RE^{3+} ions, Lutetium (Lu^{3+}) is the most suitable one to be substituted by Yb^{3+} due to a close matching of their ionic radii. Indeed, for an eight-fold oxygen coordination, $R(Lu^{3+}) = 0.977$ Å and $R(Yb^{3+}) = 0.985$ Å. This closeness of ionic radii implies low distortions of the crystalline lattice and good optical quality. Thus, $Yb:KLu(WO_4)_2$ and $Yb:LuVO_4$ crystals are very promising for the development of efficient and high reliable Yb lasers.

Efficient $Yb:KLu(WO_4)_2$ and $Yb:LuVO_4$ lasers working in the continuous-wave (CW) [9, 10], Q-switched [11] and mode-locked [12,13] operation modes were reported previously. In particular, passive Q-switching (PQS) of a solid-state laser with a saturable absorber (SA) is a commonly used method to produce ns-long pulses from a compact and reliable all-solid device that does not require external control like for the active Q-switching. Recently, novel types of SAs based on carbon nanostructures (e.g., graphene and carbon nanotubes) emerged as suitable absorbers for PQS.

Graphene is a two- dimensional material composed of a single layer of carbon atoms arranged in a honeycomb lattice. It shows relatively strong linear absorption (2.3% for a single-layer) with a weak wavelength dependence [14] as well as absorption saturation that is of practical use for PQS and mode-locking [15]. Graphene SAs exhibit a high damage threshold, low saturation intensity and ultrafast carrier dynamics [16,17]. To date, graphene SAs have been used for PQS of Yb lasers basically in the waveguide [18-20] and fiber [21-23] configurations. Although generation of sub-100 ns pulses was demonstrated, pulse energies remained relatively low (typically, tens of nJ).

In the present paper, we aimed to realize compact $Yb:KLu(WO_4)_2$ and $Yb:LuVO_4$ lasers passively Q-switched with a graphene-SA. Graphene PQS of bulk Yb lasers can provide significant improvement of the pulse energy, while the use of compact cavity design (including plano-plano one) is beneficial for the reduction of the pulse duration. In addition, using graphene high pulse repetition frequencies are possible up to the MHz-level.

2. Experimental

Two laser crystals were studied, namely Yb:KLu(WO_4)$_2$ (or Yb:KLuW) and Yb:$LuVO_4$. The Yb:KLuW crystal was grown by the Top-Seeded Solution Growth Slow-Cooling (TSSG-SC) method using a *b*-oriented seed. It was 3 at.% Yb doped (the actual ion density N_{Yb} measured with Electron Probe MicroAnalysis, EPMA, was 1.80×10^{-20} at/cm^3). The active element from this crystal was cut along the N_g optical indicatrix axis and it was 1.5 mm-thick. Both 3×3 mm^2 $m\times p$ faces of the element were polished to laser quality and remained uncoated. The Yb:$LuVO_4$ crystal was grown by the conventional Czochralski method along the *a*-axis. It was 1.5 at.% Yb doped ($N_{Yb} = 2.04\times10^{-20}$ at/cm^3). The 2.0 mm-thick active element was *a*-cut and its faces, 3.3(*c*)×3.3 mm^2, were polished but remained uncoated. The active elements were mounted in a copper holder water-cooled to 12°C using Indium foil to improve the thermal contact. The parameters of the studied laser crystals are summarized in Table 1.

The chosen Yb doping levels are typical for KLuW and $LuVO_4$ host crystals. In the particular case of Yb:$LuVO_4$, low doping is required to maintain a good crystal quality. For both materials, the chosen doping ensured uniform heat distribution under diode pumping and prevented their stress fracture.

The laser cavity consisted of a flat pump mirror (PM) antireflection (AR) coated for 0.9–1.0 μm and high-reflection (HR) coated for 1.02–1.20 μm, and a flat or concave (R = 50 mm) output coupler (OC) with transmission, T_{OC} = 5% or 10% at the laser wavelength. A commercial transmission-type graphene saturable absorber (SA) from Graphene Supermarket was inserted at normal incidence between the crystal and the OC. The SA consisted of a 1.05 mm-thick fused silica substrate with a single-layer graphene deposited by the chemical vapor deposition (CVD) method. The clean face of the substrate was uncoated. The initial transmission of the graphene-SA at the laser wavelength, T (substrate + graphene) / T (substrate) = 97.8%, Fig. 1(a). This agrees well with the universal transmission of a single-layer graphene, $T = 1 - \pi\alpha \approx 97.7\%$ (α is the fine structure constant). The characterization of this sample with Raman spectroscopy indicates a ratio of the integrated areas of the 2D and G bands of ~4, confirming the presence of a single carbon layer [24], Fig. 1(b). The air gaps between PM, laser crystal, SA and OC were all below 0.5 mm thus resulting in a total geometrical cavity length of ~4 mm. The cavity configuration with the flat or concave OC will be called plano-plano or plano-concave, respectively. The laser operating with the plano-plano cavity represented the first step to the true microchip set-up. In this case, all cavity elements were placed in contact with each other without air gaps.

The laser crystal was pumped by a fiber-coupled (fiber core diameter: 200 μm, N.A.: 0.22) InGaAs laser diode at ~978 nm. The lens assembly with imaging ratio 1:1 provided a pump spot radius in the crystal of w_p = 100 μm; the confocal parameter $2z_R$ was 3.2 mm. The total absorption in the crystal amounted to 29% for Yb:KLuW and 51% for Yb:$LuVO_4$. No bleaching of the crystal absorption was observed under unpolarized pumping. A fast (200 ps) InGaAs photodiode and 2 GHz Tektronix DPO5204B digital oscilloscope were used for detection of the Q-switched pulses.

3. Results and discussion

First, let us discuss the choice of the laser cavity geometry for Q-switching experiments. Although graphene shows almost wavelength-insensitive linear absorption from ~0.5 μm up to at least ~3 μm (~2.3%), its nonlinear properties shows strong dispersion. In particular, the saturation intensity I_{sat} increases with the photon energy hv and, as a result, I_{sat}(1 μm) is almost twice higher than I_{sat}(2 μm) [16]. Thus, deep saturation of graphene-SA in Yb laser requires special efforts by providing high intracavity intensity which can be reached by the reduction of the size of the laser mode on the SA. Second, due to very low saturable absorption (~0.1%), the typical pulse durations in graphene Q-switched lasers are from few hundreds of ns to few μs. The improvement of this parameter requires a reduction of the cavity roundtrip time. Compact plano-concave and plano-plano cavities can provide the generation of ns Q-switched pulses, as well as small size of the laser mode on the SA.

The input-output dependences for the PQS regime of the Yb:KLuW and Yb:$LuVO_4$ lasers are presented in Fig. 2(a). The laser emission was linearly polarized, $E \parallel N_m$. For the plano-concave cavity, stable PQS was achieved with both OCs. For T_{OC} = 10%, the maximum average output power of 170 mW was achieved with a slope efficiency η = 12% (with respect to the absorbed pump power, P_{abs}). The laser threshold was at P_{abs} = 1.6 W and the Q-switching conversion efficiency with respect to the CW mode η_{conv} (when the SA was removed from the cavity) amounted to 22%. For 5% OC, the laser performance was deteriorated. The maximum output power only reached 81 mW and η = 7%. In the plano-plano cavity configuration, stable PQS was achieved only for T_{OC} = 10%. The maximum output power was 113 mW and the slope efficiency was η = 6%, that is lower than for the plano-concave cavity, however, the laser threshold was reduced to P_{abs} = 1.2 W.

For the Yb:$LuVO_4$ laser, stable PQS was achieved for all the studied cavity configurations, see Fig. 2(b). The emission from this laser was linearly polarized, $E \parallel c$ (π-polarized) which agrees with previous results with *a*-cut Yb:$LuVO_4$ active elements [10]. The best results in terms of the output power (310 mW) and slope efficiency (17%) corresponded to the plano-plano cavity and T_{OC} = 10%. The Q-switching conversion efficiency was 37%. The laser threshold however was at ~4.0 W which is attributed to the inferior crystal quality (as compared with Yb:KLuW). For 5% OC, a similar level of output power was achieved (300 mW) with a reduced η = 10%. For the plano-concave cavity, the results were inferior. Indeed, for T_{OC} = 10% or 5%, the Yb:$LuVO_4$ laser generated only 155 mW with η = 9% or 169 mW with η = 5%, respectively. Modeling of the performance of Yb:KLuW and Yb:$LuVO_4$ lasers yielded ~4% round-trip loss for the graphene SA that limited the Q-switching conversion efficiency, in addition to the loss related to the Fresnel reflection from an uncoated substrate. As it will be shown later this corresponded to non-saturable loss in the graphene SA.

For both Yb:KLuW and Yb:$LuVO_4$ lasers, an upper limit for stable PQS existed: the laser cavity was still stable and no drop of the output power was observed, however it was difficult to achieve a stable train of Q-switched pulses. It was observed at P_{abs} ~3 W for Yb:KLuW laser and ~6.2 W for Yb:$LuVO_4$. It corresponded to the same level of residual (non-absorbed) pump power, ~5 W. Intensity instabilities in graphene Q-switched compact lasers are attributed to the heating of the SA due to the residual pump [25]. A mismatch of the thermal expansion coefficients

for graphene and substrate (fused silica) [26] causes a compressive strain in the graphene layer with rising temperature and can, in principle, lead to its slip or buckling from the substrate surface. This can lead to a spatially non-uniform increase of the non-saturable losses in graphene-SA. However, no damage of the graphene-SA was observed in our experiments.

The emission spectra from the Yb:KLuW and Yb:$LuVO_4$ lasers are shown in Fig. 3. For both lasers, the spectra consisted of a single narrow (full width at half maximum, FWHM < 0.5 nm) emission line that was centered at 1030 or 1032 nm for Yb:KLuW and 1021 or 1024 nm for Yb:$LuVO_4$ (for T_{OC} = 5 or 10%, respectively). The observed blue-shift of the emission wavelength with the increase of output coupling is typical for quasi-three-level Yb lasers and it is in accordance with the gain spectra [1]. The spectra were clearly different from those in CW regime where a multi-peak behavior was observed.

For Yb:KLuW, the shortest Q-switched pulses were obtained with the plano-concave cavity and T_{OC} = 10%. The corresponding dependence of the pulse duration (FWHM) and pulse repetition frequency (PRF) is shown in Fig. 4(a). With the increase of pump level from 1.6 to 2.9 W of absorbed power, the pulse duration shortened from ~800 to 165 ns (this dependence shows a saturation for P_{abs} >2.5 W) and the PRF increased nearly linearly from 60 to 350 kHz. The saturation of the pulse duration dependence is attributed to the nearly complete saturation of the graphene-SA. The use of 5% OC provided slightly longer pulses, 210 ns at PRF = 320 kHz. For the Yb:KLuW laser with the plano-plano cavity (using T_{OC} = 10%), 280 ns pulses were achieved at a PRF of 240 kHz. For the Yb:$LuVO_4$ laser, the shortest Q-switched pulses (152 ns, PRF = 360 kHz) were generated using the plano-plano cavity configuration and T_{OC} = 5%, see Fig. 4(b). Similar pulse characteristics (165 ns / 340 kHz) were detected for this OC using the plano-concave cavity. For 10% OC, much longer pulses were achieved.

The oscilloscope records of the shortest Q-switched pulses and the corresponding pulse trains obtained for Yb:KLuW and Yb:$LuVO_4$ lasers are shown in Fig. 5. The intensity instabilities in the pulse trains were ~15%. This value is determined by the above mentioned heating of graphene-SA. An asymmetric shape of the single pulses indicates that the ratio between the initial transmission of the graphene-SA (that can be varied by the number of graphene layers n) and the output coupler transmission can be further optimized.

By using the data on the average output power, PRF and pulse duration, we calculated the pulse energies ($E_{out} = P_{out}$/PRF) and peak powers ($P_{peak} = E_{out}/\tau$) for the Yb:KLuW and Yb: $LuVO_4$ lasers. For the Yb:KLuW laser with a plano-concave cavity, the maximum pulse energy reached 0.49 μJ and it corresponded to a maximum peak power of 3.0 W (T_{OC} =10%). Yb:$LuVO_4$ laser with the plano-plano cavity provided a nearly 2-fold increase of the two parameters, 0.94 μJ / 3.9 W and 0.84 μJ / 5.5 W for T_{OC} = 10% and 5%, respectively. The pulse energy and peak power dependences on the absorbed pump power for the described lasers are presented in Fig. 6. The peak power increased nearly linear with P_{abs}, while the pulse energy was saturated at high pump levels, probably due to the heating of the SA.

A summary of the PQS performance of Yb:KLuW and Yb:$LuVO_4$ lasers is presented in Table 2.

The different behavior of Yb:KLuW and Yb:$LuVO_4$ lasers for plano-concave and plano-plano cavity configurations can be explained considering the intracavity peak intensity on the SA,

I_{in}. In order to calculate I_{in}, we considered the spatial and temporal distribution of the laser beam. In the assumption of TEM_{00} laser mode and nearly Gaussian temporal profile of single pulses, $I_{in} = X[2E_{out}/\pi w_l^2 \tau^*]$, where $X = (1+R)/(1-R)$ and R is the reflectivity of the OC, w_l is the radius of the laser mode, the term "2" indicates Gaussian spatial profile and $\tau^* \approx 1.06\tau$ is the effective pulse duration. To estimate the value of the laser waist (w_l), first we calculated the sensitivity factor of the thermal lens [27], $M = 2.1$ and 3.7 m^{-1}/W for Yb:KLuW and $Yb:LuVO_4$ crystals, respectively. Thus, the value of w_l for the plano-plano/plano-concave cavities was ~61/42 μm (for Yb:KLuW) and ~44/38 μm (for $Yb:LuVO_4$), respectively, that was always below the radius of the pump beam, w_p. The results on I_{in} are then summarized in Table 3. The values I_{in} should be compared with the typical value of saturation intensity for CVD-grown single-layer graphene, I_{sat} ~0.7–1 MW/cm^2 at ~1 μm [16].

For the Yb:KLuW laser with a weaker thermal lens than $Yb:LuVO_4$, the use of concave OC has a significant effect on the laser mode and, hence, on the intracavity intensity. For Yb:KLuW laser with the plano-plano cavity, I_{in} ~0.6 MW/cm^2 that is slightly below the I_{sat} value. However, for the plano-concave cavity, I_{in} is ~2 times higher than the saturation intensity. This means stronger bleaching of the SA and, consequently, generation of shorter pulses, see Table 2. For the $Yb:LuVO_4$ laser with a stronger lens, both flat and concave OCs provide similar size of the laser mode (that is rather small) and, consequently, similar intracavity intensity values, about ~2.5 and 5–7 MW/cm^2 for 10% and 5% OC, respectively. Both these values are much higher than the saturation intensity, so almost complete bleaching of the graphene-SA for the $Yb:LuVO_4$ laser is expected. It also explains the generation of shorter pulses with higher energies for this laser.

To model the characteristics of our graphene Q-switched lasers, we have solved the system of rate equations for a quasi-three-level laser material and fast saturable absorber:

$$\frac{dI_l}{dt} = \frac{c\mu}{n}[k_l - k_L - \frac{1}{l_a}\alpha_{SA}(I_l)]I_l + I_{noise}, \quad (1a)$$

$$\frac{dN_2}{dt} = \frac{I_p}{h\nu_p}k_p - \frac{I_l}{h\nu_l}k_l - \frac{N_2}{\tau}. \quad (1b)$$

Here, we have introduced two variables: (i) I_l – radiation intensity in the laser crystal at the laser frequency ν_l and (ii) N_2 - population of the upper laser level ($N_1 + N_2 = N_{Yb}$, where N_1 is the population of the ground-state and N_{Yb} is the concentration of Yb^{3+} ions). Both of these variables are considered as averaged over the crystal length and over the transverse dimensions. The remaining parameters are as follows: c is the light velocity, $\mu = l_a n/l_c$ is the resonator filling factor; l_a is the active element length; n is the refractive index of the active element; l_c is the optical length of the resonator, $k_l = N_2\sigma_l - N_{Yb}\sigma^l_{abs}$ is the gain coefficient at the laser frequency ν_l ($\sigma_l = \sigma^l_{SE} + \sigma^l_{abs}$, σ^l_{SE} and σ^l_{abs} are the stimulated-emission (SE) and absorption cross-sections of the active material at the laser frequency ν_l, respectively), $k_L = -[\ln(1-T_{OC})+\ln(1-L)]/(2l_a)$ is the resonator loss coefficient, where T_{OC} is the transmission of the output coupler and L is the round trip passive intracavity loss, α_{SA} is the loss coefficient in the saturable absorber, I_{noise} is the noise rate, $I_p = I^p_{inc}[(1-\exp(-k_p l_a))/k_p l_a]$ is the average pump intensity ($I^p_{inc} = P_{inc}/\pi w_p^2$ is the incident pump intensity, P_{inc} is the incident pump power and w_p is the pump spot radius), h is the Planck constant, ν_p is

the pump frequency, $k_p = N_{Yb}\sigma^p_{abs} - N_2\sigma_p$ is the absorption coefficient for the pump radiation ($\sigma_p = \sigma^p_{SE}+\sigma^p_{abs}$, σ^p_{SE} and σ^p_{abs} are the SE and absorption cross-sections of the active material at the pump frequency ν_p, respectively), τ is the lifetime of the upper laser level ($^2F_{5/2}$ level of Yb^{3+}).

The saturable absorption of graphene is typically described as [15,16]:

$$\alpha'_{SA}(I_l) = \alpha'_{NS} + \frac{\alpha'_S}{1+(I_l/I_{sat})}, \qquad (2)$$

where α'_{NS} and α'_S are the non-saturable and saturable absorption of graphene, respectively (where the absorption, α', and transmission, T, are related as $\alpha' = 1 - T$, and $\alpha'_{NS} + \alpha'_S = 1 - T_{SA}$, T_{SA} is the initial transmission of the graphene-SA) and I_{sat} is the saturation intensity for graphene-SA. As already mentioned, for our graphene sample, the initial absorption was 2.2%. For the modeling, the saturation intensity of a single-layer graphene at ~1 μm was taken as 1.0 MW/cm^2 [16]. Typically for a single-layer graphene, α'_S is considered to be 1.5% [16]. However, our calculations for the lasers studied here indicated that the saturable absorption of the used graphene sample is lower, ~0.2%. This explains the relatively high insertion loss for the graphene related to high non-saturable absorption.

The solution of Eq. (1) yielded a time-dependent intracavity laser intensity $I_l(t)$ which was used to calculate the output laser power, $P_{out}(t) = I_l(t)V_lk_{act}$, where $V_l = l_a\pi w_l^2/2$ is the volume of the laser mode in the active element (w_l is the radius of the laser mode) and k_{act} is the coefficient of the saturable losses, $k_{act} = -[\ln(1-T_{OC})]/(2l_a)$. From the time-dependent $P_{out}(t)$, we have calculated the pulse duration (as FWHM), the pulse energy and the PRF for the Q-switched pulses. The material parameters of Yb:KLuW and Yb:$LuVO_4$ (absorption and SE cross-sections, refractive indices and $^2F_{5/2}$ lifetime) used for the modeling are listed in Table 4. The results from the calculations are shown as solid curves in Fig. 4 and Fig. 6. The used model provides rather good agreement with the experimental data. The largest deviation of the calculated data from the experimental ones is observed for PRF which is lower than expected from modeling. However, the latter correctly represents the pulse energies. Thus, the modeling predicts the generation of higher average output power (P_{out} = PRF·E_{out}) than observed in the experiment. We refer this to the temperature variation of the spectroscopic properties of the laser crystal which can lead to the drop in laser output.

The developed Yb:KLuW and Yb:$LuVO_4$ lasers with a plano-plano cavity represent the first step to Yb microchip lasers passively Q-switched with graphene. For these lasers, the stabilization of the laser mode is provided by the positive thermal lens ($M > 0$). Although positive sign of the thermal lens is inherent for tetragonal vanadates due to the positive thermo-optic coefficients (dn/dT) [5], the positive thermal lens for Yb:KLuW (with $dn/dT < 0$) is provided by the special crystal cut along the N_g-axis. For this crystal cut, positive impact of thermal expansion of the laser element compensates negative impact of dn/dT [28]. It should be noted that in our previous work on graphene PQS of Yb:YAG [29], the attempt to build a Q-switched microchip laser failed mainly due to the weak positive thermal lens in this crystal, with M ~1.7 m^{-1}/W, and, hence, the weak mode confinement in the cavity was not enough to bleach the graphene SA and thus a curved output coupler had to be used.

In Table 5, we compare the performance of graphene-SA Q-switched Yb lasers developed previously and in the present work. With a Yb:Y_2O_3 waveguide laser, sub-100 ns pulses were

achieved, however with a much lower pulse energy (0.08 μJ) [20] than in the present work. Later on in [30], this result was improved, generating 158 ns / 0.33 μJ pulses. Low pulse energies were due to a very high PRF reaching the MHz level. Yb fiber lasers permit optimization of either pulse duration or energy but not both, so the achieved parameters, 70 ns / 0.046 μJ [21] or 1600 ns / 0.65 μJ [23], are not comparable with our results with bulk lasers in terms of peak power.

Further optimization of graphene-SA Q-switched compact Yb lasers is possible with the use of multi-layered graphene (n = 2…4) that can provide an increased modulation depth and, hence, shorten the pulses to ~10 ns with pulse energy reaching >10 μJ, as it can be expected from the modeling. In particular, the compactness of the laser cavity is clearly beneficial when using graphene because it allows for a reduction of the pulse duration with respect to the standard hemispherical cavities by a factor of ~10, as recently shown for graphene-SA Q-switched Tm:KLuW microchip laser [25]. The microchip lasers also offer the possibility of direct deposition of graphene on the crystal face without the need of additional focusing. An important question for power scaling is then the reduction of the unwanted heating of the SA by the residual pump that is inherent to the microchip design. This can be done by increasing the Yb-doping concentration which is possible for the KLuW crystal.

Improvement of the quality of the graphene-SA is essential for minimization of its insertion loss and, thus, to increase the laser slope efficiency. In our experiments, both laser crystals were uncoated. This did not affect the Q-switched laser performance (it just contributed to the passive intracavity losses). However, AR-coatings on crystal surfaces will potentially improve the laser efficiency.

4. Conclusions

We report on bulk Yb lasers passively Q-switched with a single-layer graphene SA. It is shown that although graphene possesses a high saturation intensity at ~1 μm, it can be used to provide stable PQS of Yb lasers when using a compact laser set-up (including the microchip-like configuration), as well as active materials with a strong thermal lens. These are the factors that can provide deep bleaching of the SA due to a strong mode confinement, and generation of nanosecond pulses both due to the reduction of the cavity roundtrip time and to the above mentioned deep bleaching. With the compact (~4 mm-long), diode-pumped Yb:KLuW and Yb:$LuVO_4$ lasers, we achieved 165 ns / 0.49 μJ and 152 ns / 0.83 μJ pulses, respectively. The maximum average output power from the Yb:$LuVO_4$ laser with the plano-plano cavity reached 310 mW at 1021 nm with 17% slope efficiency (corresponding to 240 ns pulses and a PRF of 330 kHz). Further improvement of the output characteristics of graphene Q-switched Yb lasers is expected with the use of multi-layered graphene.

Acknowledgements

This work was supported by the Spanish Government under projects MAT2013-47395-C4-4-R and TEC2014-55948-R, and by the Generalitat de Catalunya under project 2014SGR1358. F.D. acknowledges additional support through the ICREA academia award 2010ICREA-02 for excellence in research. This work is part of a project that has received funding from the European

Union's Horizon 2020 research and innovation programme under the Marie Skłodowska-Curie grant agreement No 657630.

References

1. V. Petrov, M.C. Pujol, X. Mateos, O. Silvestre, S. Rivier, M. Aguiló, R.M. Solé, J. Liu, U. Griebner, F. Díaz: Laser & Photon. Rev. 1, 179 (2007).
2. V. E. Kisel, A. E. Troshin, N. A. Tolstik, V. G. Shcherbitsky, N. V. Kuleshov, V. N. Matrosov, T. A. Matrosova, M. I. Kupchenko: Opt. Lett. 29, 2491 (2004).
3. J. Petit, B. Viana, P. Goldner, D. Vivien, P. Louiseau, B. Ferrand: Opt. Lett. 29, 833 (2004).
4. Y. Sato, T. Taira: Opt. Express 14, 10528 (2006).
5. P.A. Loiko, K.V. Yumashev, V.N. Matrosov, N.V. Kuleshov: Appl. Opt. 52, 698 (2013) [Erratum: Appl. Opt. 54, 4820 (2015)].
6. M. C. Pujol, M. A. Bursukova, F. Guell, X. Mateos, R. Solé, Jna. Gavaldà, M. Aguiló, J. Massons, F. Díaz, P. Klopp, U. Griebner, V. Petrov: Phys. Rev. B 65, 165121 (2002).
7. J.M. Serres, P. Loiko, X. Mateos, K. Yumashev, N. Kuleshov, V. Petrov, U. Griebner, M. Aguiló, F. Díaz: Opt. Mater. Express 5, 661 (2015).
8. S. Rivier, X. Mateos, Ò. Silvestre, V. Petrov, U. Griebner, M. C. Pujol, M. Aguiló, F. Díaz, S. Vernay, D. Rytz: Opt. Lett. 33, 735 (2008).
9. J. Liu, V. Petrov, X. Mateos, H. Zhang, J. Wang: Opt. Lett. 32, 2016 (2007).
10. J. Liu, V. Petrov, H. Zhang, J. Wang, M. Jiang: Opt. Lett. 31, 3294 (2006).
11. J. Liu, V. Petrov, H. Zhang, J. Wang: Appl. Phys. B 88, 527 (2007).
12. S. Rivier, X. Mateos, J. Liu, V. Petrov, U. Griebner, M. Zorn, M. Weyers, H. Zhang, J. Wang, M. Jiang: Opt. Lett. 14, 11668 (2006).
13. U. Griebner, S. Rivier, V. Petrov, M. Zorn, G. Erbert, M. Weyers, X. Mateos, M. Aguiló, J. Massons, F. Díaz: Opt. Exp. 13, 3465 (2005).
14. R.R. Nair, P. Blake, A.N. Grigorenko, K.S. Novoselov, T.J. Booth, T. Stauber, N.M.R. Peres, A.K. Geim: Science 320, 1308 (2008).
15. Q. L. Bao, H. Zhang, Y. Wang, Z. Ni, Y. Yan, Z. X. Shen, K. P. Loh, D. Y. Tang: Adv. Funct. Mater. 19, 3077 (2009).
16. F. Zhang, S. Han, Y. Liu, Z. Wang, X. Xu: Appl. Phys. Lett. 106, 091102 (2015).
17. G. Xing, H. Guo, X. Zhang, T. C. Sum, C. H. A. Huan: Opt. Express 18, 4184 (2010).
18. A. Choudhary, S. Dhingra, B. D'Urso, P. Kannan, D.P. Shepherd: IEEE Phot. Technol. Lett. 27, 646 (2015).
19. J.W. Kim, S.Y. Choi, S. Aravazhi, M. Pollnau, U. Griebner, V. Petrov, S. Bae, K.J. Ahn, D.-I. Yeom, F. Rotermund: AIP Advances, 5, 017110 (2015).
20. A. Choudhary, S. Dhingra, B. D'Urso, T.L. Parsonage, K.A. Sloyan, R.W. Eason, D.P. Shepherd: Opt. Lett. 39, 4325 (2014).
21. J. Liu, S. Wu, Q.-H. Yang, P. Wang: Opt. Lett. 36, 4008 (2011).
22. L. Zhang, J. T. Fan, J. H. Wang, J. M. Hu, M. Lotya, G. Z. Wang, R. H. Li, L. Zhang, W. J. Blau, J. N. Coleman, J. Wang, Y. Feng: Laser Phys. Lett. 9, 888 (2012).
23. L. Zhang, Z. Zhuo, R. Wei, Y. Wang, X. Chen, X. Xu:Chin. Opt. Lett. 12, 021405 (2014).
24. A.C. Ferrari, J.C. Meyer, V. Scardaci, C. Casiraghi, M. Lazzeri, F. Mauri, S. Piscanec, D. Jiang, K.S. Novoselov, S. Roth, A.K. Geim: Phys. Rev. Lett. 97, 187401 (2006).

25. J. M. Serres, P. Loiko, X. Mateos, K. Yumashev, U. Griebner, V. Petrov, M. Aguiló, F. Díaz: Opt. Express 23, 14108 (2015).
26. D. Yoon, Y. W. Son, H. Cheong: Nano Lett. 11, 3227 (2011).
27. P. Loiko, F. Druon, P. Georges, B. Viana, K. Yumashev: Opt. Mater. Express 4, 2241 (2014).
28. P.A. Loiko, J.M. Serres, X. Mateos, K.V. Yumashev, N.V. Kuleshov, V. Petrov, U. Griebner, M. Aguiló, F. Díaz: Laser Phys. Lett. 11, 125802 (2014).
29. J. M. Serres, V. Jambunathan, X. Mateos, P. Loiko, A. Lucianetti, T. Mocek, K. Yumashev, V. Petrov, U. Griebner, M. Aguiló, F. Díaz: IEEE Photonics J. 7, 1503307 (2015).
30. A. Choudhary, S.J. Beecher, S. Dhingra, B. D'Urso, T.L. Parsonage, J.A. Grant-Jacob, P. Hua, J.I. Mackenzie, R.W. Eason, D.P. Shepherd: Opt. Lett. 40, 1912 (2015).

Figure captions

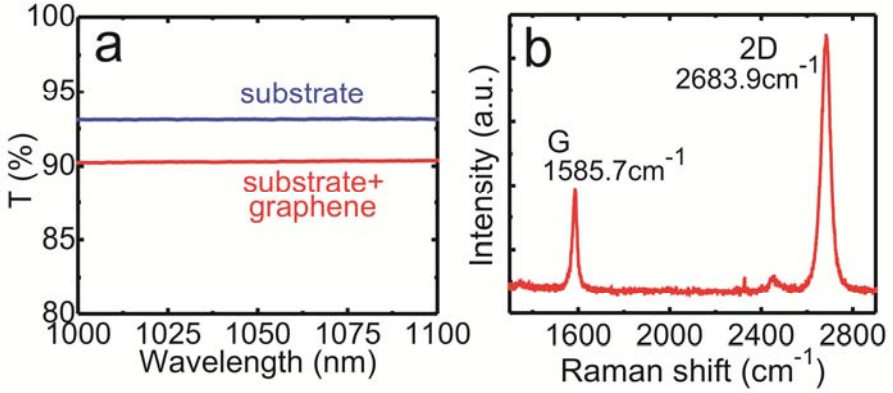


Figure 1 Characterization of the graphene-SA: (a) transmission spectrum, T(substrate+graphene)/T(substrate) = 97.8%. (b) Raman spectrum.

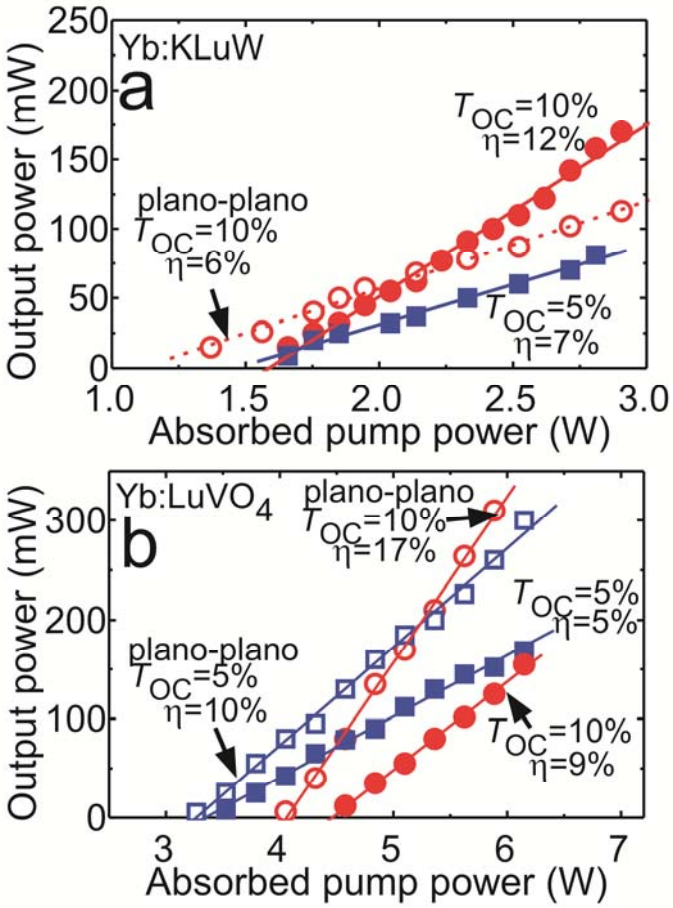


Figure 2 Input-output dependences of the graphene-SA passively Q-switched lasers: (a) Yb:KLuW and (b) Yb:$LuVO_4$: *open* symbols – plano-plano cavity, *filled* symbols – plano-concave cavity, *lines* are the fitting of the experimental data for the slope (η) calculation.

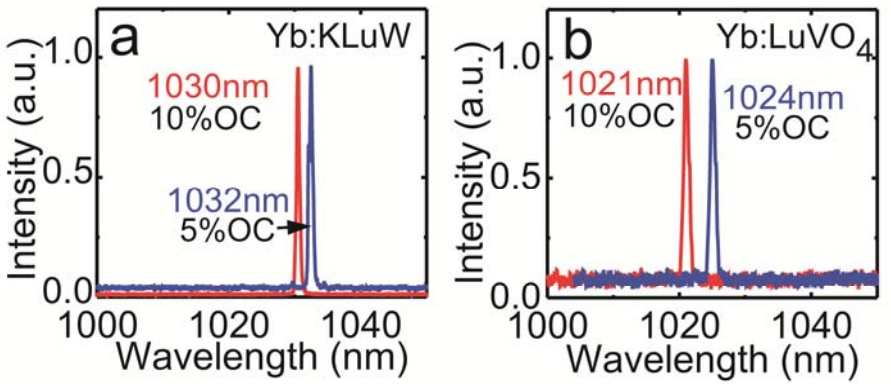


Figure 3 Emission spectra of the graphene-SA passively Q-switched lasers: (a) Yb:KLuW (P_{abs} = 2.9 W), and (b) Yb:$LuVO_4$ (P_{abs} = 6.1 W, plano-concave cavity).

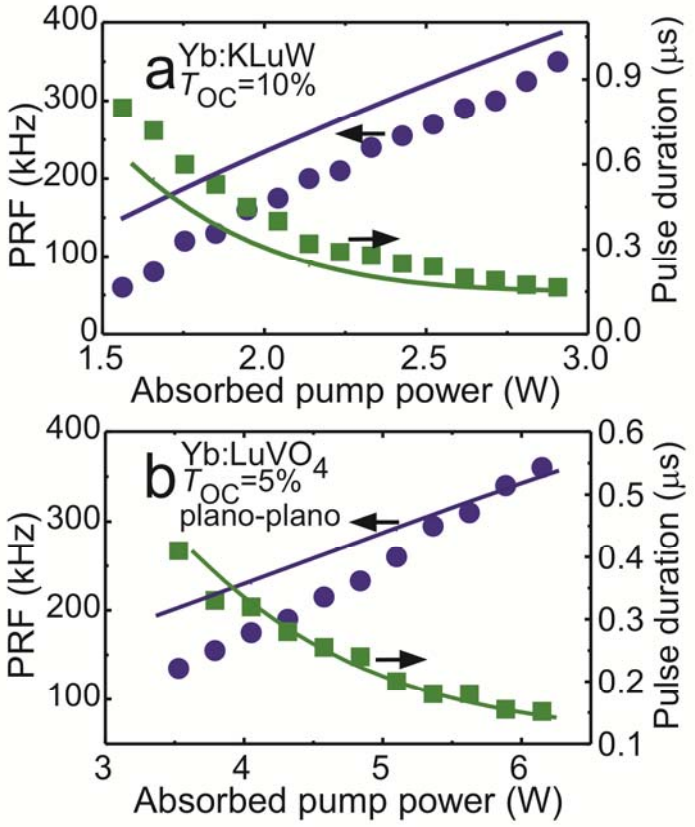


Figure 4 Pulse duration (FWHM) and pulse repetition frequency (PRF) of the graphene-SA passively Q-switched (a) Yb:KLuW laser (T_{OC} = 10%), (b) Yb:$LuVO_4$ laser with the plano-plano cavity (T_{OC} = 5%); *symbols* are the experimental data, *curves* refer to the modeling.

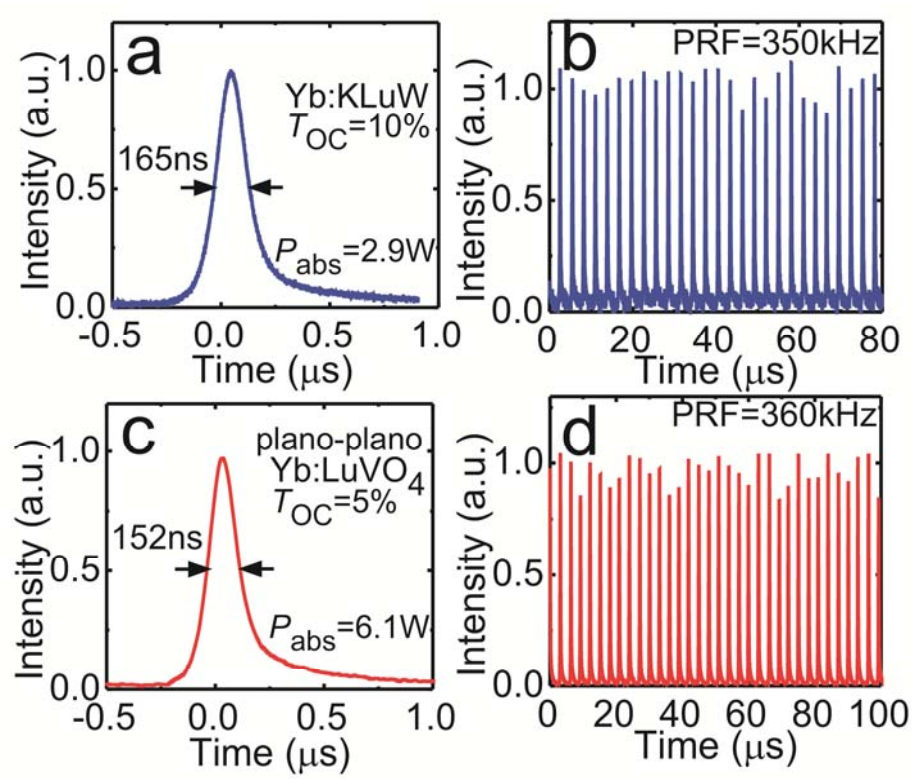


Figure 5 Single pulse and pulse train records for graphene-SA passively Q-switched (a,b) Yb:KLuW laser with the plano-concave cavity (T_{OC} = 10%) and (c,d) $Yb:LuVO_4$ laser with the plano-plano cavity (T_{OC} = 5%).

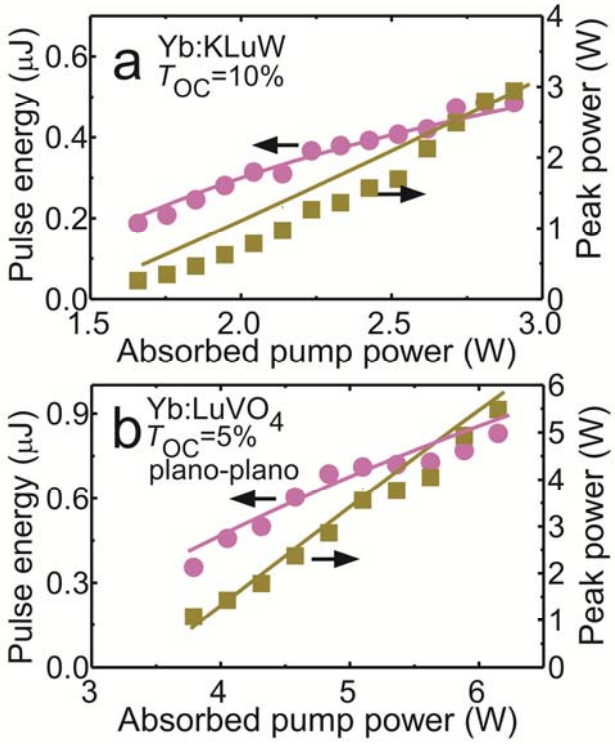


Figure 6 Pulse energy and peak power of the graphene-SA passively Q-switched (a) Yb:KLuW laser with the plano-concave cavity (T_{OC} = 10%), (b) $Yb:LuVO_4$ laser with the plano-plano cavity (T_{OC} = 5%): *symbols* are the experimental data, *curves* refer to the modeling.

Table 1 Parameters of the studied Yb:KLuW and Yb:$LuVO_4$ crystals.

Parameter	Yb:KLuW	Yb:$LuVO_4$
Growth method	TSSG	Czochralski
Crystal class	monoclinic / biaxial	tetragonal / uniaxial
Yb doping	3.0 at.%	1.5 at.%
N_{Yb}, 10^{-20} at/cm^3	1.80	2.04
Crystal cut	N_g-cut	a-cut
Aperture, mm^2	3.0(m)×3.0(p)	3.3(c)×3.3
Thickness, mm	1.5	2.0

Table 2 Output characteristics* of the Yb:KLuW and Yb:$LuVO_4$ lasers passively Q-switched with a single-layer graphene-SA.

Cavity	T_{OC}	P_{th}, W	P_{out}, mW	η, %	η_{conv}, %	τ, ns	PRF, kHz	E_{out}, μJ	P_{peak}, W
Yb:KLuW									
Plano-concave	10%	1.6	170	12	22	165	350	0.49	3.0
	5%	1.5	81	7	7	210	320	0.25	1.2
Plano-plano	10%	1.2	113	6	13	280	240	0.47	1.7
	5%	Unstable PQS							
Yb:$LuVO_4$									
Plano-concave	10%	4.6	155	9	35	190	270	0.57	3.0
	5%	3.5	169	5	19	165	340	0.50	3.0
Plano-plano	10%	4.0	310	17	37	240	330	0.94	3.9
	5%	3.2	300	10	28	152	360	0.83	5.5

*P_{th} – laser threshold, P_{out} – output power, η – slope efficiency, η_{conv} – Q-switching conversion efficiency, τ – pulse duration, PRF – pulse repetition frequency, E_{out} – pulse energy, P_{peak} – peak power.

Table 3 Mode-matching analysis and intracavity peak intensity for graphene Q-switched Yb:KLuW and Yb:$LuVO_4$ lasers.

Crystal	M, m^{-1}/W	w_p, μm	Cavity	w_l, μm	I_{in}(5%OC), MW/cm^2	I_{in}(10%OC), MW/cm^2
Yb:KLuW	2.1	100	Plano-concave	42±5	1.6	2.0
			Plano-plano	61±5	–	0.6
Yb:$LuVO_4$	3.7	100	Plano-concave	38±5	5.2	2.5
			Plano-plano	44±5	7.0	2.5

Table 4 Material properties of Yb:KLuW and Yb:$LuVO_4$ used for modeling of the Q-switched laser performance, in accordance with [1,10].

Parameter*	Notation	Unit	Yb:KLuW ($E \parallel N_m$)	Yb:$LuVO_4$ ($E \parallel c$)
Absorption cross-section	σ^p_{abs} / σ^l_{abs}	10^{-20} cm^2	3.0 / 0.2	3.1 / 0.2
SE cross-section	σ^l_{SE} / σ^p_{SE}	10^{-20} cm^2	2.3 / 3.2	1.4 / 3.0
Refractive index	n		2.0294	2.249
Lifetime of the $^2F_{5/2}$ state	τ	μs	275	256

* Superscripts "p" and "l" correspond to the values at the pump and laser wavelengths, respectively.

Table 5 Comparison of the output characteristics of the current Yb-lasers passively Q-switched with graphene-SA.

Laser / type	P_{out}, mW	η, %	τ, ns	PRF, kHz	E_{out}, μJ	Ref.
Yb:$KY(WO_4)_2$ / waveguide	34	9	349	607	0.059	[19]
Yb:Y_2O_3 / waveguide	83	25	98	1040	0.080	[20]
Yb:Y_2O_3 / waveguide	456	13	158	1470	0.33	[30]
Yb:glass / waveguide	21	3	140	833	0.027	[18]
Yb / fiber	12	–	70	257	0.046	[21]
Yb / fiber	16	–	1300	110	0.142	[22]
Yb / fiber	35	–	1600	55	0.65	[23]
Yb:$KLu(WO_4)_2$ / bulk	170	12	165	350	0.49	This work
Yb:$LuVO_4$ / bulk	300	10	152	360	0.83	This work
Yb:YAG / bulk	185	12	228	285	0.65	[29]